Electronic supporting Information

Threshold Switching Memristor-based Stochastic Neuron for Probabilistic Computing

Kuan Wang, ‡[a] Qing Hu, ‡[a] Bin Gao,[b] Qi Lin,[a] Fu-Wei Zhuge,[c] Da-You Zhang,[a] Lun Wang,[a] Yu-Hui He,*[a] Ralph H. Scheicher,[d] Hao Tong*[a] and Xiang-Shui Miao*[a]

[a] Wuhan National Laboratory for Optoelectronics, School of Optical and Electronic Information, Huazhong University of Science and Technology, Wuhan 430074, China

E-mail: heyuhui@hust.edu.cn, tonghao@hust.edu.cn, miaoxs@hust.edu.cn

[b] Institute of Microelectronics, Tsinghua University, Beijing 100084, China.

[c] The State Key Laboratory of Material Processing and Die & Mould Technology, School of Materials Science and Engineering, Huazhong University of Science and Technology, Wuhan 430074, China

[d] Division of Materials Theory, Department of Physics and Astronomy, Uppsala University, Uppsala SE-75120, Sweden

‡ These authors contributed equally to this work.

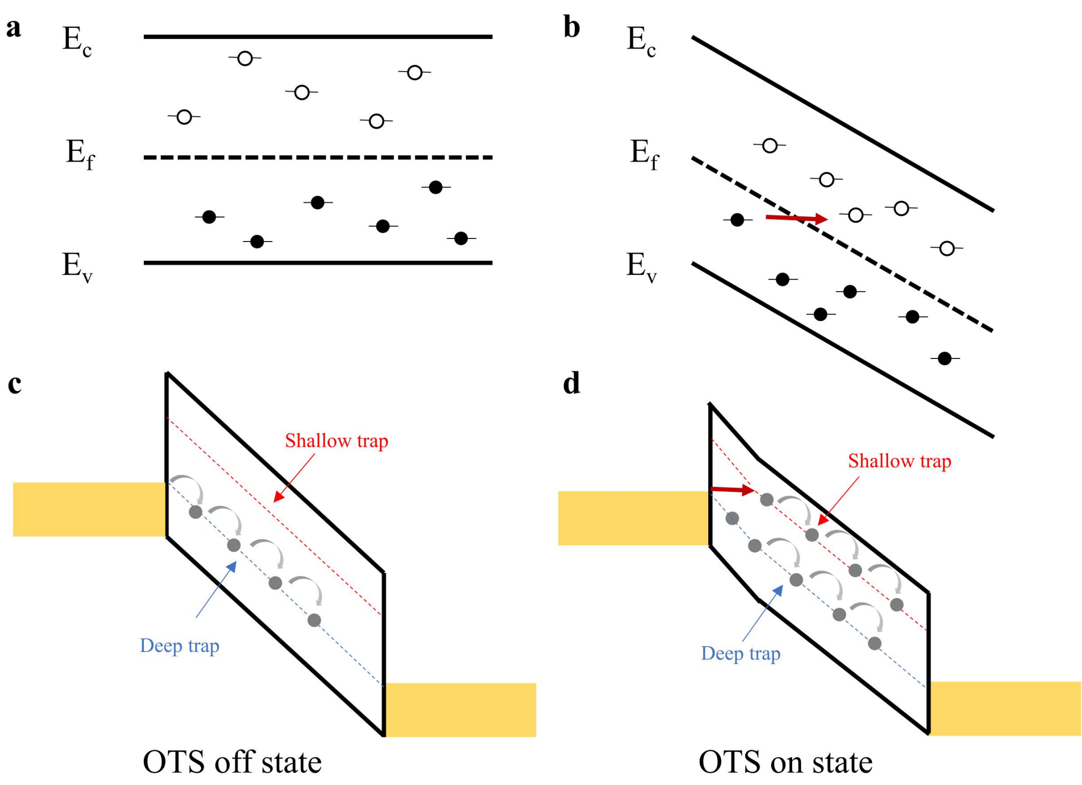

Fig. S1 Schematic diagram of the transition mechanism of OTS devices. Distribution of electrons (a) before, and (b) after voltage is applied. In the absence of an imposed electric field, the trap states below the Fermi level are occupied while those above it are not. By applying the voltage, the energy band gets bent and the Poole-Frenkel conduction model now describes the I-V characteristics (c) at small voltage and (d) at large voltage.[1] While staying within the deep trap states below the Fermi level under small voltage, the electrons would jump between the traps, allowing those empty shallow trap states at higher energies to be accessed through thermal emission or tunneling processes. The kinetic energy gained by one electron under the high electric field can be shared among a larger number of excited electrons. Thus a large electric field can lead to a non-equilibrium distribution of carriers and non-uniform electric field distribution along the film, which allows for the abrupt conductivity switching.

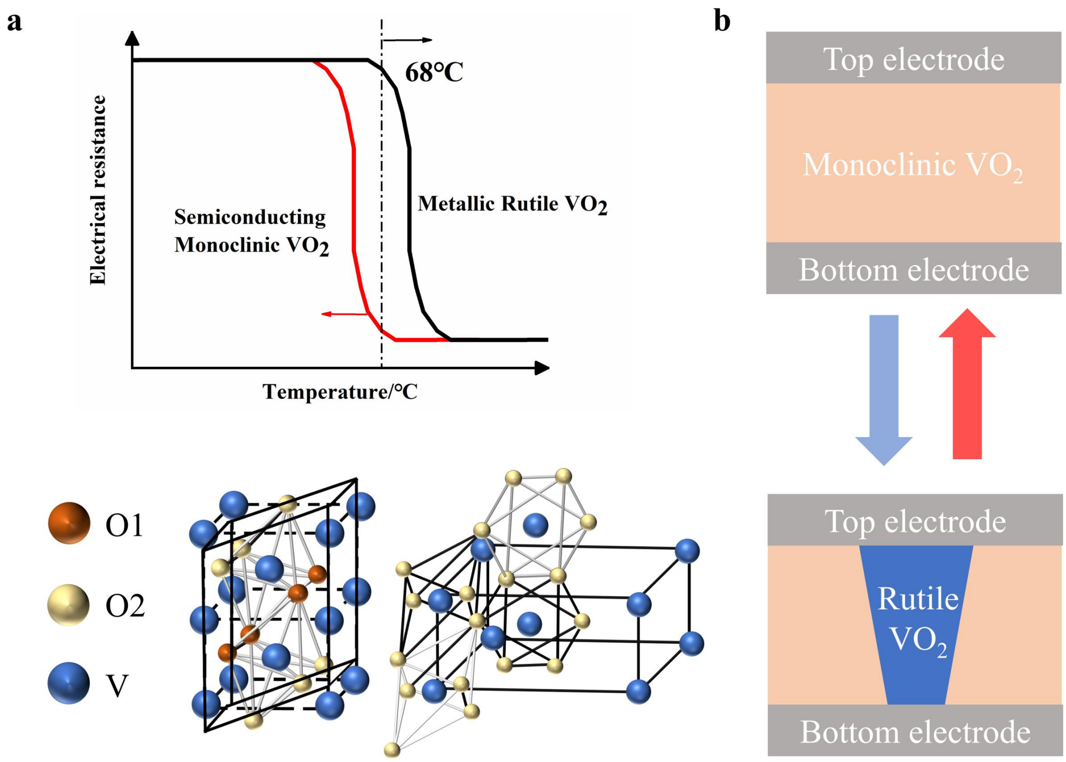

Fig. S2 Schematic diagram of the transition mechanism of VO_2 devices. (a) The electrical resistance of the VO_2 device versus temperature and the structural transition in VO_2.[2] Under applied electric field or high temperature, the VO_2 crystal could be transformed from a monoclinic structure to a rutile structure. (b) Threshold switching in VO_2 devices. The electrical conductivity of two types of crystal structure known as monoclinic and rutile is quite different. Upon the transition of partial VO_2 from monoclinic to rutile, a high conductance channel is formed between the top and bottom electrodes, resulting in the switching from high-resistance state (HRS) to low-resistance state (LRS). By removing the applied electric field, VO_2 relaxes to its original monoclinic state, thus returning to the HRS.

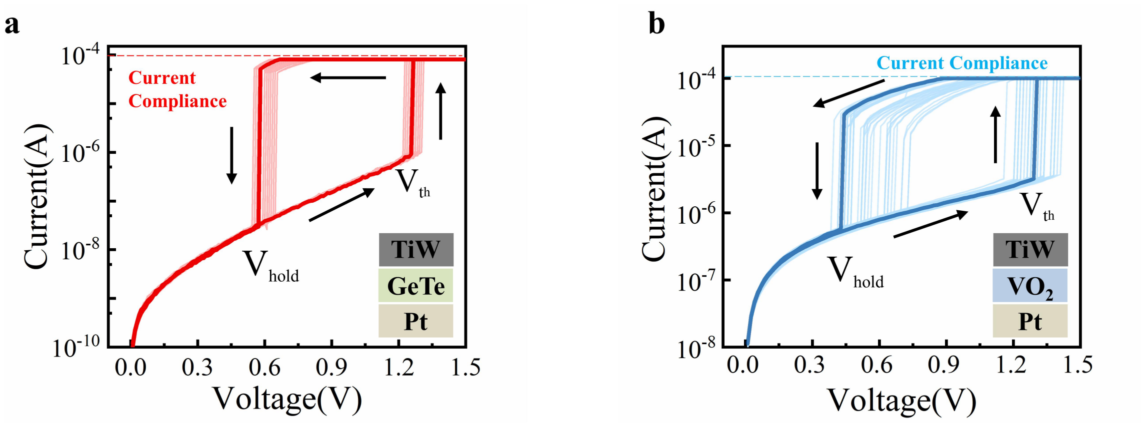

Fig. S3 Stochastic threshold switching behavior observed in TSM devices. Consecutive DC switching cycles of the TSM devices under current compliance measured in **(a)** $GeTe_6$ (OTS), **(b)** VO_2 (MIT).

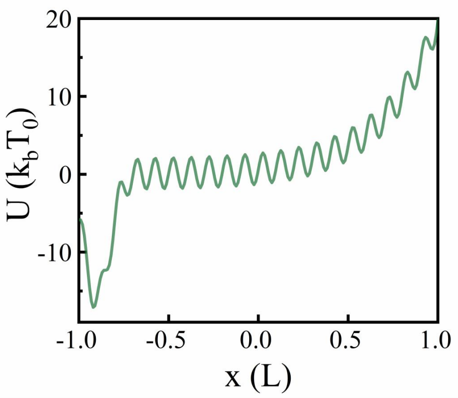

Fig. S4 Electric potential normalized by thermal energy used for the particle simulation. It is composed by two types of energy with quite different scales. One is the interfacial energy responsible for detaching the CuS layer and the other is the much weaker nanoparticle-pinning energy with many smaller wells between the electrodes.

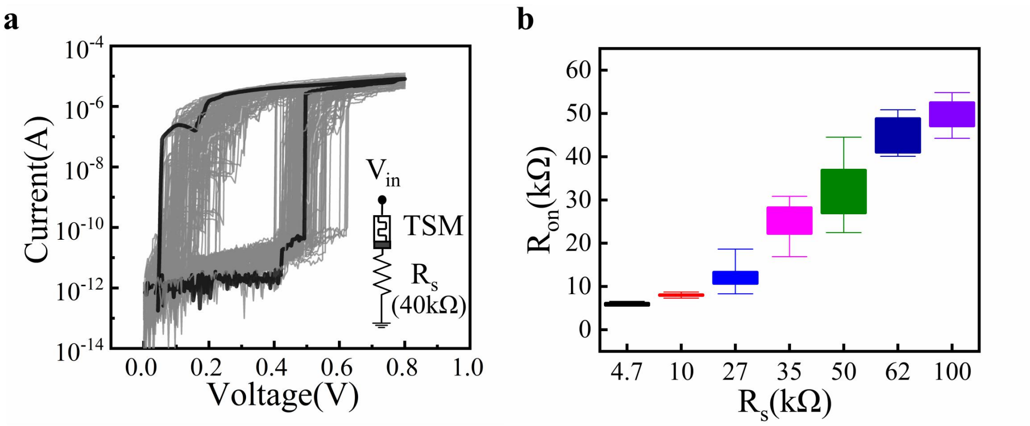

Fig. S5 Electrical characteristics of CuS/GeSe-based CBTS with series resistors. (a) 100 Consecutive DC switching cycles of the CuS/GeSe device connected to a 40 kΩ series resistor. The cycle to cycle variation of the threshold voltage V_{th} shows favorable stochasticity for fabricating the demanded neurons without compliance currents. (b) The measured R_{on} of the CuS/GeSe device connected in series with a resistor R_s with various amounts of resistance.

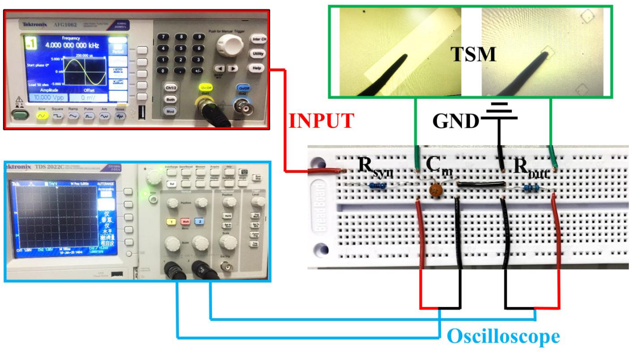

Fig. S6 Stochastic neuron test platform. The neuron circuit test platform is built on a breadboard, where TSM devices are accessed through a probe station and the voltage changes inside the circuit are monitored by an oscilloscope.

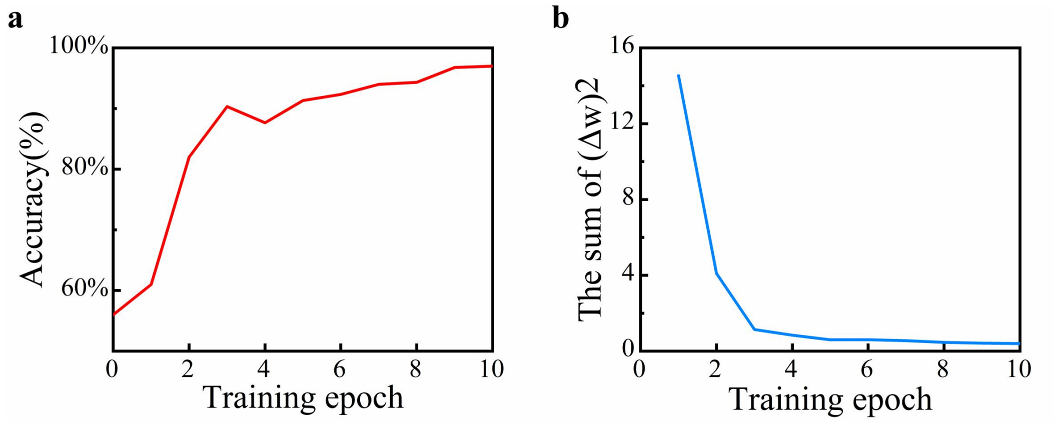

Fig. S7 The training process of probabilistic SNN. (a) Prediction accuracy during training epoch. The highest accuracy of probabilistic SNN neural network is 97.0%. (b) The change of sum of $(\Delta w)^2$ during training epochs. The synaptic weight tuning of the network becomes convergent after 10 training epochs.

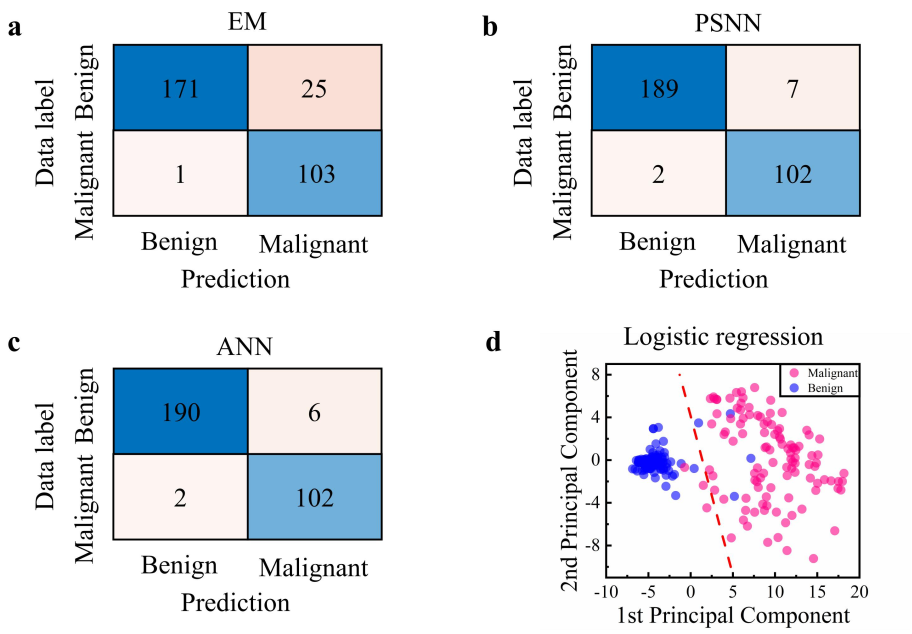

Fig. S8 Comparison of Probabilistic SNN and EM(Expectation-Maximum) algorithm recognition results. Confusion matrixes of prediction results of 300 test breast cancer data by (a) Expectation-Maximum (EM) algorithm (b) probabilistic spiking neural network (PSNN) and (c) artificial neural network (ANN). (d) Decision boundary (red line) and classification result of logistic regression after PCA analysis. The ANN and logistic regression are supervised learning, while the probabilistic SNN and EM algorithm are unsupervised learning. The probabilistic SNN here achieves accuracy of 97.0% comparing to 91.3% by the EM algorithm, 97.3% by the ANN and 97.6% by logistic regression after PCA.

TABLE I

Reference	Device type	Reset Circuit	Stochastic	Application
[3]	CMOS	Yes	No	Not referred
[4]	PCM	Yes	Yes	Temporal correlations detection
[5]	RRAM	Yes	Yes	MNIST
[6]	FEFET	Yes	No	MNIST
[7]	MTJ	Yes	Yes	MNIST
[8]	TSM (VO_2)	No	Yes	MNIST
[9]	TSM ($Ag/SiO_2/Au$)	No	Not referred	MNIST
[10]	TSM (VO_2)	No	Yes	Not referred
Our work	TSM (CuS/GeSe)	No	Yes	Probabilistic computation (Cancer diagnosis)

Table S1 | Summary of artificial neurons based on various technology choices.

TABLE II

Types of CBTS	**MIT**	**OTS**	**CBTS**
Material	VO_2	GeTe	CuS/GeSe
On-off ratio	$>10^2$	$>10^2$	$>10^9$
R_{off}	~500 kΩ	~1 MΩ	~1 GΩ
Leakage current	$\sim10^{-6}$ A	$\sim10^{-8}$ A	$\sim10^{-12}$ A
V_{th} range	0.4 V~1.1 V	1.2 V~1.3 V	0.3 V~0.7 V
V_{hold} range	0.1 V~0.3 V	0.5 V~0.7 V	0 V~0.2 V
Standard deviation of V_{th}	0.156 V	0.020 V	0.076 V

Table S2 | Comparison of three types of TSM devices electrical parameters. The same via-hole structures with diameter 250 nm and depth 100 nm have been used for three types of CBTS devices in order to quantitatively evaluate and compare their performance.

TABLE III

Simulation parameters of probabilistic SNN	**Symbol**	**Simulation value**
Time step of simulation	α	0.1ms
Potentiation factor of STDP	c	0.05
Depression factor of STDP	b	0.001
Time window of STDP	σ	50ms
Maximum weight	w_{max}	2
Minimum weight	w_{min}	0
Input spiking rate	v	40Hz
Input time duration of each data	-	50ms
Firing probability	$P_f(u)$	$\exp[9.08 * (u - 0.5133)] / 0.7547$

Table S3 | Simulation parameters of probabilistic SNN for cancer diagnosis. The input is encoded as that given $f_i = j$ ($1 \leq j \leq 10$), the input neuron X_{ij} will fire with a spiking rate v_{ij} = 40Hz, while the rest of the population remain silent ($X_{ij'}$=0 if $j' \neq j$). The output neurons response is calculated using the experimentally measured dependence of the firing probability on the membrane potential $u_k(t)$, and $P_f(u)$= $\exp[9.08 * (u - 0.5133)]/0.7547$.

Supplementary Reference：

1. D. Ielmini and Y. Zhang, *Journal of Applied Physics*, 2007, **102**, 054517.
2. M. M. Qazilbash, M. Brehm, B.-G. Chae, P.-C. Ho, G. O. Andreev, B.-J. Kim, S. J. Yun, A. Balatsky, M. Maple and F. Keilmann, *Science*, 2007, **318**, 1750-1753.
3. G. Indiveri, 2003.
4. T. Tuma, A. Pantazi, M. Le Gallo, A. Sebastian and E. Eleftheriou, *Nature nanotechnology*, 2016, **11**, 693.
5. M. Al-Shedivat, R. Naous, G. Cauwenberghs and K. N. Salama, *IEEE journal on Emerging and selected topics in circuits and systems*, 2015, **5**, 242-253.
6. Z. Wang, B. Crafton, J. Gomez, R. Xu, A. Luo, Z. Krivokapic, L. Martin, S. Datta, A. Raychowdhury and A. I. Khan, 2018.
7. A. Sengupta, P. Panda, P. Wijesinghe, Y. Kim and K. Roy, *Scientific reports*, 2016, **6**, 30039.
8. M. Jerry, A. Parihar, B. Grisafe, A. Raychowdhury and S. Datta, 2017.
9. X. Zhang, W. Wei, L. Qi, Member and IEEE, *IEEE Electron Device Letters*, 2018, **39**, 308-311.
10. W. Yi, K. K. Tsang, S. K. Lam, X. Bai, J. A. Crowell and E. A. Flores, *Nature Communications*, 2018, **9**.